In vivo diabetic wound healing with nanofibrous scaffolds modified with gentamicin and recombinant human epidermal growth factor

Charu Dwivedi[1,2], Ishan Pandey[3], Himanshu Pandey[2,4], Sandip Patil[5], Shanti Bhushan Mishra[6],Avinash C Pandey[2], Paolo Zamboni[7],Pramod W Ramteke[1]*,Ajay Vikram Singh[8]*

[1]Department of Biological Sciences, Sam Higginbottom University of Agriculture, Technology and Sciences, Allahabad- 211007 (India)

[2]Nanotechnology Application Centre, Faculty of Science, University of Allahabad, Allahabad-211002 (India)

[3]Department of Clinical Laboratory Science, Sam Higginbottom University of Agriculture, Technology and Sciences, Department of Microbiology Motilal Nehru Medical College, (MLNMC) ALLAHABAD-211001 (INDIA)

[4]Department of Pharmaceutical Sciences, Faculty of Health Sciences, Sam Higginbottom University of Agriculture, Technology & Sciences, Allahabad- 211007 (India)

[5]Indian Institute of Technology (IIT) Kanpur- 208016

[6]United Institute of Pharmacy, Allahabad- 211002 (India)

[7]Vascular Disease Center, University of Ferrara, Italy.

[8]Physical Intelligence Department, Max Planck Institute for Intelligent Systems, Stuttgart 70569, Germany

*E-mail: avsingh@is.mpg.de, pwramteke@gmail.com.

Abstract

Diabetic wounds are susceptible to microbial infection. The treatment of these wounds requires a higher payload of growth factors. With this in mind, the strategy for this study was to utilize a novel payload comprising of Eudragit RL/RS 100 nanofibers carrying the bacterial inhibitor gentamicin sulphate (GS) in concert with human epidermal growth factor (rhEGF); an accelerator of wound healing. GS containing Eudragit was electrospun to yield nanofiber scaffolds, which were further modified by covalent immobilization of rhEGF to their surface. This novel fabricated nanoscaffold was characterized using scanning electron microscopy

This article has been accepted for publication and undergone full peer review but has not been through the copyediting, typesetting, pagination and proofreading process which may lead to differences between this version and the Version of Record. Please cite this article as an 'Accepted Article', doi: 10.1002/jbm.a.36268

(SEM), Fourier Transform Infrared (FTIR) Spectroscopy and X-ray diffraction (XRD). The thermal behavior of the nanoscaffold was determined using thermogravimetric analysis and differential scanning calorimetry. In the*in vitro* antibacterial assays, the nanoscaffolds exhibited comparable antibacterial activity to pure gentemicin powder. *In vivo* work using female C57/BL6 mice, the nanoscaffolds induced faster wound healing activity in dorsal wounds compared to the control. The paradigm in this study presents a robust *in vivo* model to enhance the applicability of drug delivery systems in wound healing applications.

Keywords: Wound healing, *in vivo*, rhEGF, nanofibrous scaffolds, electrospinning

1. Introduction

Diabetes mellitus is a serious impedance on chronic wound healing, furthermore the pathophysiology of diabetic ulcers is complex[1].Inadequate management and treatment of chronic wounds leads to a reduction in physical activity and amputation of affected limbs[2]. Diabetic patients are susceptible to impaired wound healing; this process wound repair and tissue regeneration relies on the extracellular matrix (ECM), which recruits progenitor cells to the wound bed[3].The ECM is prone to changes that are brought on by tissue damage and injury. Cells in the body restore the ECM integrity by cell-cell and cell-matrix interactions via cross-talk between different factors in the angiogenic/coagulation cascade[4]. Infection is a common occurrence in diabetic ulcers, additionally there is a correlation between improper wound healing and infection. The leading cause of gangrene and amputations is attributed to diabetic wounds that become infected during the course of therapy with antibiotics[5,6]. Anaerobic bacteria in diabetic foot ulcers can develop into deep-wound if the infection spreads into deeper tissue[7]. Management of such wounds is complicated by looming antibody resistance due to multidrug resistant organisms[8].

The current approach to epidermis engineering revolves around three dimensional (3D) scaffold fabrication that not only can mimic the ECM but also provide mechanical support for cells,the means of local release of biomolecules that facilitate tissue regeneration and assists diabetic wound healing[9-11].The placement of acellular scaffolds immediately after trauma to the skin facilitates the regulated release of biomolecules. These in turn initiates the recruitment of progenitor cells to defective areas and cause cellular proliferation, and differentiation[12].In the last

decade, the use of nanomaterials in biomedical applications has increased due to their comprehensive assortment of implementations [13-15]. Their popularity is due to noticeable virtues such as their dimension (10-100 nm scale), physicochemical and biological characteristics. Their physical state (i.e. nanoparticle, quantum dots, nanocrystals nanotubes and nanofibers) and furthermoretheir properties such as high reactivity, large surface-to-mass ratio and ultra-small size make them high useful in biomedical application[16-18].

The use of electrospinning technology is a very promising solution for the mass production of thin nanofibers with good conformability and usage as scaffolds for tissue engineering/regeneration[19]. Nanomaterials possess smart properties such as: larger surface area, small diameter, high porosity, and a 3D web structure. These properties can be utilized to improve the functions of other incorporated materials. Furthermore this can also lead to the gain of additional functions due to quantum effects[20].The surface modification of electrospun nanofibers or biofunctionalization leads to the alteration of cytocompatibility of nanofibers. Biomolecules such as growth factors and ECM proteins can be incorporated into nanofiber scaffolds during electrospinning or post processing through adsorption[21,22].

In an attempt to design a dual nanocarrier system that eliminates infection and promote diabetic wound healing, a functional 3D Eudragit RL/RS 100 nanofibrous scaffold was fabricated. The scaffold surface was modified by the application of GS and rhEGF by utilizing electrospinning and covalent immobilization respectively. The rationale for this approach was with reference to a drug eluting stent. This new scaffolds was characterized and analyzed using *in vivo* approach. In the present scenario, tunable and controlled release of the antibacterial in conjunction with the wound healingwas achieved. This novel dual drug delivery system allows for the synchronous release of GS and rhEGF and may serve as faster, and efficient therapy for the treatment of diabetic ulcers.

2. Materials and methods

2.1 Materials

Eudragit RL and RS 100 (Evonik, Germany), GSsulphate (FDC India Ltd., Mumbai), Polyethylene glycol (PEG-400), methanol, nutrient broth andnutrientagar (Merck Specialties Pvt. Ltd. Mumbai), N, N-dimethylacetamide (DMAc), suberic acid bis(N-hydroxy-succinimideester) (NHS), bovine serum albumin (BSA), 1,6-diaminohexane and 2,2-dihydroxyindane-1,3-dione

(ninhydrin) (LobaChemie Pvt. Ltd. Mumbai). rhEGF (Recombinant human epidermal growth factor) (Life Technologies India Pvt. Ltd., New Delhi). All other chemicals and reagents were of analytical grade.

2.2 Composite nanoscaffold fabrication

Eudragit polymer solution (20%) was prepared by dissolving equal quantities of Eudragit RL 100 and RS 100 polymers in 5:1 (v/v) methanol: DMAc. Thereafter, 5 mg/ml GS sulphate (GS) was added to the prepared polymer solution. 2 ml of PEG-400 was also added to the solution. The polymer solution was loaded into 5 ml syringes and was electrospun into nanofibrous scaffolds using an in-house electrospinning setup. A blunt-ended 20-gauge stainless steel needle was used as the nozzle. The emitting electrode from a Gamma High Voltage Research ES30P power supply capable of generating DC voltages was attached to the needle. A rotating disc wrapped with a piece of aluminum foil collected the ultrafine aligned nanofibers. The obtained electrospun nanofibrous scaffolds were dried at room temperature under vacuum to remove organic solvent and moisture (Figure 1). The processing conditions for nanoscaffold fabrication are listed in Table 1.

2.3 Modification of composite nanoscaffolds with rhEGF

Covalent immobilization technique was used to immobilize the growth factor rhEGF on the surface of the fabricated nanofibrous scaffolds by the covalent immobilization technique[23]. In brief, the scaffold pieces (20 mm in diameter) were first aminolyzed by soaking them in a 10% (w/v) solution of 1,6-hexanediamine in isopropanol. The scaffolds were incubated at room temperature for 3 hr and subsequently washed in PBS (pH 7.4) five times. They were then washed with 70% ethanol and PBS. The scaffolds were thereafter immersed in 10 ml PBS containing 0.08 mmol NHS with gentle agitation for 4 hr at room temperature and proceeded with a five times PBS wash. The now active scaffolds, were immersed in 10 μg/ml rhEGF solutions in PBS with gentle shaking for 12 hr at 4°C. The rhEGF-immobilized scaffolds were subjected to a final PBS washed and freeze-dried.

2.4 Physicochemical characterization of rhEGF immobilized composite nanoscaffolds.

2.4.1 Surface topography

The morphology and surface features of the electrospun rhEGF-Composite nanoscaffolds was observed by a Hitachi-4800 scanning electron microscope (SEM). Before examination, the samples were adhered to SEM studs, and then coated with gold using a sputter-coater (EMITECH K550X) for 4 min at 30 mA.

2.4.2 Fourier Transform Infrared Spectroscopy

Chemical characteristics were determined by Fourier Transform Infrared Spectroscopy, using a Nicolet-Nexus 670 FTIR spectrophotometer. All spectra were recorded using a transmission mode with a wavenumber range of 450–4000 cm^{-1} at room temperature.

2.4.3 X-Ray Diffraction

The crystalline structure of the nanoscaffolds was characterized by Spinner PW3064 XPERT-PRO X-ray diffraction system using Cu Kα radiation with continuous scanning at 40 mA, 45 kV. The scan was performed from 5° to 60° (2θ). The plane spacing of different diffraction planes (d_{hkl}) can be calculated from Bragg's Law (equation 1):

$$d_{hkl} = \frac{\lambda}{2 \sin \theta} \quad (1)$$

Where λ is the wavelength of the copper anode source (λ = 1.54 Å) and θ stands for the diffraction angle of each indexed diffraction plane.

2.4.4 Thermal properties

The thermal properties of the nanoscaffolds were evaluated using Thermogravimetric Analysis (TGA) and Differential Scanning Calorimetry (DSC). TGA was performed in an automated thermal analyzer system(Diamond TG/DTA 8.0, Perkin-Elmer, USA). Sealed samples were heated in an aluminum pan at a temperature of 20 °C/min,50 °C and 900 °C under a constant nitrogen flow rate of 150 ml/min through the sample chamber. The DSC measurements were carried out in the same instrument, however the temperature range was from -50°C to 300°C at a heating rate of 15°C/min under a nitrogen atmosphere.

2.5 Biological characterization of rhEGF immobilized composite nanoscaffolds

2.5.1 Quantification of rhEGF

In order to confirm the presence of amine groups on the surface of the developed nanoscaffolds treated with 1,6-hexanediamine, ninhydrin assay was performed[24,25]. The scaffold (diameter 15 mm) was treated with a 1.0 M solution of ninhydrin prepared in ethanol for 1 min and then transferred to a glass vial that was heated for 15 min at 70°C. The treated scaffold was dissolved

in 2 ml tetrahydrofuron (THF) and isopropanol each. The obtained solution was placed in a silica cuvette and the optical density was measured at 560 nm using a Lambda 25 UV−Vis spectrophotometer (Perkin-Elmer, USA). The amount of amine groups on the scaffold was quantified by plotting a standard curve in the range of 5-25 μg/ml using 1,6-hexanediamine solutions in isopropanol. Further, the amount of immobilized rhEGF was determined by measuring the fluorescence intensity of tryptophan group present on rhEGF immobilized nanofibrous scaffolds. The rhEGF assay was performed at 280 nm excitation and 342 nm emission wavelengths using a fluorescence spectrophotometer (Perkin Elmer Model – LS 45) then, the rhEGF intensity remaining in solution at the end of the immobilization process was subtracted from the initial amount of rhEGF in the immobilization solution which was equivalent to the amount of immobilized rhEGF.

2.5.2 Degree of swellingand Porosity

The swelling behavior of the nanoscaffolds was calculated by immersing them in PBS (pH 7.4) for 24 hr at room temperature[26]. After 24 hr, the scaffold was removed and the excess buffer solution was wiped with filter paper and weighed. The weights were recorded and the degree of swelling was calculated using equation 2.

$$Degree\ of\ swelling(\%) = \frac{w - w_0}{w_0} \times 100 \quad (2)$$

Where, w= weight of scaffold after immersion and w_0= weight of scaffold before immersion.

The porosity of the nanoscaffolds was measured using the gravimetry method[27].The thicknesses of the scaffold was measured using microcallipers and then the apparent density ($\rho_{scaffold}$) and porosity (ε) were calculated equations 3 and 4:

$$\rho_{scaffold} = \frac{Mass\ of\ scaffold}{Thickness\ of\ scaffold \times Area\ of\ scaffold} \times 100 \quad (3)$$

$$\varepsilon = 1 - \frac{\rho_{scaffold}}{\rho_{material}} \quad (4)$$

Where, $\rho_{material}$ is the density of bulk PLGA.

2.5.3 Water contact angle

Water contact angle measurements were performed using an FTA1000 instrument (FirstTenÅngstroms Inc.). Measurements were obtained using MilliQ water (3 nanoliters) on different ns-TiOx/ZrOx gradient spots. The mean value was obtained from five individual measurements. To ensure statistical validity, each measurement of a contact angle was recorded in 150 images in a 5 second time frame using a Pelco camera (model PCHM 575-4). The standard deviation was approximately 2°. Image analysis was performed by the FTA Windows Mode 4 software.

2.6 Polymer-drug profile

Drug entrapment efficiency, drug loading capacity and *invitro* drug release studies were used as parameters to study the polymer-drug profile in the composite nanoscaffolds. A drug assay was carried out to determine the drug entrapment capacity of the GS loaded nanofibrous scaffolds as reported in our previous study[28].

Drug loaded nanofibrous scaffolds were placed in PBS (pH 7.4) and centrifuged at 8000 rpm for 5 min. Thereafter,3 ml of ninhydrin reagent was added to the supernatant and the absorbance was measured using a Lambda 25 UV−vis spectrophotometer (Perkin-Elmer, USA) at 566 nm. The amount of drug in the sample was calculated using the standard curve prepared from PBS. The drug entrapment efficiency was calculated by comparing with the amount of drug used to prepare the nanofibrous scaffolds according to equation 5:

$$Drug\ Entrapment\ Effiecency\ (\%) = \frac{M}{M_0} \times 100 \quad (5)$$

Where, M = mass of entrapped drug and M_0 = mass of drug used in formulation

The drug loading capacity is the ratio of the mass of bound drug to the mass of the scaffold and was calculated using equation 6.

$$Drug\ Loading\ Capacity\ (\%) = \frac{F}{W} \times 100 \quad (6)$$

In vitro drug release was studied using the membrane diffusion method as previously described[29,30].In brief, the GS loaded scaffolds were incubated in 5 ml of aqueous buffer solution at a pH gradient of 3, 7.4 and 9 respectively. The diffusion medium was sampled (1 ml volume) at hourly time points (total time 12hr) and replaced with an equal quantity of fresh diffusion medium. The final analyte comprised of diffusion medium and ninhydrin reagent (total volume

10 ml). Absorbance was measured using a Systronics 10 UV-Vis spectrophotometer at a wavelength of 566 nm. The control used consisted of ninhydrin agent only.

2.7*In vitro* antibacterial activity

The antibacterial activity of composite nanoscaffolds was evaluated against *Staphylococcus aureus*; a Gram-positive bacteria in solid medium[31,32].The bacteria strain was obtained from the Microbiology Department, Sam Higginbottom Institute of Agriculture, Technology and Science, Allahabad. Nutrient agar plates were prepared by autoclaving nutrient agar media and pouring onto petri dishes and air dried. Nutrient broth reconstituted aliquots of bacteria (100 ml) were spread on agar plates. GS -free and GS -containing PLGA/Gelatine 70:30 and PLGA/Gelatine 50:50 nanofibrous scaffolds were cut into circular discs (15 mm in diameter) and placed on the top of the agar plate. The plates were incubated at 37°C for 24 hr. The absence of bacteria growth was indicative of inhibitory concentration being reached. This was visually characterized by clear zone around the scaffold specimens. The presence of this zone was used as a marker for identifying inhibition of the bacteria.

Antibacterial activity was further determined using liquid media[31].The bacterial culture was grown in nutrient broth. Thereafter absorbance was measured at 625 nm. When readings of 0.1-0.2 were reached, 5ml samples of the culture were transferred to test tubes. Drug loaded nanofibrous scaffolds were then inserted into these tubes. Samples were incubated at 37°C for 24 hr with in a shaker incubator. The positive control used was GS powder, the negative control lacked scaffolds; an additional negative control was also used containing cotton gauze.

Absorbance readings were carried out at 625 nm using UV-Vis spectroscopy. All experiments were conducted in triplicate. The percentage of bacterial inhibition was calculated using the equation below:

$$\text{Bacterial Inhibition (\%)} = \frac{I_C - I_S}{I_C} \times 100 \qquad (7)$$

Where $I_C$and $I_S$are the average absorbance readings of the control group and the experimental group, respectively.

2.8 Experimental induction of diabetes

The various *in vivo* studies were performed in accordance with the Institutional Animal Ethics Committee (IAEC) constituted as per directions of the Committee for the Purpose of Control and

Supervision of Experiments on Animals (CPCSEA), under the Ministry of Animal Welfare Division, Government of India, New Delhi. The approval from the Institutional Animal Ethical Committee of Bundelkhand University, Jhansi, was taken prior to the experimental work (BU/Pharm/IAEC/13/29).Five groups of Female C57BL/6 mice weighing (14-15 g) were selected, each group having 6 mice. All animals were allowed to adapt to cages for 3 days, after which they were fasted overnight. Streptozotocin (STZ) was freshly dissolved in (0.1M, pH 4.5) citrate buffer and non-insulin-dependent diabetes mellitus was induced in overnight fasted mice by a single intraperitoneal injection of Streptozotocin (40 mg/kg by wt.). Blood glucose levels were measured 4 days after STZ injection and only mice with fasting blood glucose levels greater than 200 mg/dl were considered to be diabetic and were used in the experiment[33,34].

2.9*In vivo* wound healing studies on C57/BL6 diabetic mice

Wounds in the diabetic mice were created by following the excision wound model, whereby their dorsal hairs were shaven and an excision made with scissors and tweezer on the back of the animal. The wound areas were sterilized with povidone iodide. All treatments started 3 days after STZ injection. Five different treatments were applied in order to demonstrate wound healing. Group 1 (C)- no treatment (negative control); Group 2 (G)- positive control of pure GS solution; Group 3 (E)- Eudragit RL/RS 100 scaffold; Group 4 (EGG)-Eudragit RL/RS 100 scaffold loaded with GS and rhEGF; and Group 5 (EG)- Eudragit RL/RS 100 containing GS only.

The treatments were applied to aseptically treated wounds to determine the therapeutic effects on the wounds. After each treatment interval, the scaffolds were removed with tweezers. The wounds were photographed on day 1 and the treatment regime repeated on day 4, 8 and 12. The percentage reduction of the wound area was calculated using equation 8 below.

$$\text{Wound Area } (\%) = \frac{A}{A_i} \times 100 \quad (8)$$

Where, A_i is the initial wound area, and A is the wound area after a fixed time interval.

2.10 Statistical analysis.

Statistical analysis was conducted using a paired t-test or an unpaired, two-tailed Student's t-test. A p-value of <0.05 was considered to be statistically significant. Data are expressed as means ±

standard deviation. For the statistical validation of data, three independent experiments (n=3) were performed in triplicate.

3. Results

3.1 Physicochemical and thermal characterization of nanocomposite scaffolds

The SEM micrographs of the composite nanofibrous scaffolds are shown in Figure2A.It can be inferred that the fibers were randomly distributed and interconnected. Moreover, the fibersaresmooth without any bead formation and drug deposition on the surface. The calculated average diameter of the fibersis shown in the insert graph as a histogram and mimics the network structure of extracellular matrix. FTIR spectrum of rhEGF-GS loaded scaffold and other supplements used as control areshown in Figure 2B and supporting figure S2. The major absorption bands were recorded at 1644 and 1536 cm^{-1}, corresponds to amide I and amide II bonds found in rhEGF. The assigned minor peaks between 1635-1665 $cm^{-1}$are due to unreacted $–NH_2$ groups in GS loaded nanofibrous scaffolds. The peak was slightly deviated due to the polarity of the proximal environment. Peaks recorded between 2800-3400 cm^{-1} represented unreacted “free” hydroxyl groups within the GS structure. A comparison of the assigned peak for functional group of spectra for different component in nanofibrous scaffolds is shows in Table 2. The XRD analysis is displayed in Figure 2.C. This shows the ability of nanofibrous scaffolds to form a stable colloidal layered structure in aqueous solution, which, facilitates drug encapsulation. Additionally the scaffolds lacked distinct peaks in the displayed patterns, thereby indicating their fully amorphous nature. The characteristic peak of GS was present at 2θ of 18°. TheXRD spectra of Eudragit-RL/RS 100 scaffold, Gentamycin Sulphate + Eudragit-RL/RS 100 scaffold and Gentamycin Sulphate are shown in supporting figure S3.

The thermal properties of the nanofibrous scaffold were characterized differential scanning calorimetry and thermogravimetric analysis. The TGA data obtained are shown in Figure 3A and it shows the GS curve generated with TGA where weight loss for GS was recorded at 200°C and 330-500°C. The curves for Eudragit RL/RS 100 showed weight losses at 150 and 450°C respectively. Interestingly the TGA curves of GS loaded scaffolds exhibited weight loss at 150°C and 400-500°C and continued up to 800°C. Less than 2% weight loss below 250°C was observed, which continued up to 800ºC. Hence, GS loaded Eudragit RL/RS 100 nanofibrous scaffolds showed thermal stability compared to pure polymer and drug.

The thermograms for DSC are shown in Figure 3B. A peak at 210°C corresponds the melting point of pure GS. Another peak at 410°C was observed, however this was due to the degradation of GS. For pure Eudragit RL/RS 100 polymer the peak was observed at 240°C and attributed to the glass transition temperature (Tg) therefore indicating the amorphous nature of Eudragit RL/RS 100. With respect to GS loaded scaffolds, a peak was recorded at 420°C. This suggested that the drug stability increased due to encapsulation of the drug between polymeric chain and crystalline structure of GS.

3.2 Biochemical characterization of composite nanoscaffolds

A ninhydrin assay was used to detect the presence of amine groups on the surface of the aminolyzed scaffolds. The quantified amount of amine groups was 28 ± 1.2 µg per scaffold in Eudragit RL/RS 100 nanofibrous scaffolds. The presence of amine groups clearly indicated the success of aminolysis. Results of the quantitative analysis of rhEGF immobilization as obtained from the fluorescence spectrophotometry showed that the amount of immobilized rhEGF on Eudragit RL/RS 100 scaffolds was 4.07 ± 0.2 µg per scaffold where immobilization efficiency reached 40.7%.

The swelling behavior of the composite nanofibrous scaffolds was analyzed. The scaffolds were incubated in PBS (pH 7.4) for 24 hour at room temperature. The swelling index of scaffolds was 336 ± 3.26%. In contrast, the swelling index of cotton gauze was only 280 ± 8.64 % (Figure 3.C). In the present work, the porosity was calculated by the gravimetry method and was 76% for the composite nanofibrous scaffolds. In contrast the porosity of cotton gauze was 99.7% (Figure 3.C). The porosity was quite close to that of cotton gauze which enables the scaffolds for use in wound healing applications. The hydrophilicity of a material is indicative of its adhesive ability. The water contact angle for Eudragit RL/RS 100 nanofibrous scaffolds measured and recorded as 25.93°± 0.7 (Figure 3.D). Since this value was much less than 90°C, the scaffolds could be considered as being highly hydrophilic.

3.3Pharmacological characterization of polymer-drug profile

The drug entrapment efficiency is the ratio of the mass of drug released to the mass of total drug added. It was found to be 72.2 ± 0.74 % for composite nanofibrous scaffolds (Table 3). The drug loading capacity was found to be 2.79 ± 0.06 µg/mg^{-1} for composite nanofibrous scaffolds (Table 3).*In vitro* drug release profile of GS at different pH levels was studied (Figure 4.A) and it

revealed constant drug release and absence of burst effect therefore indicating the homogeneous dispersion of the polymeric matrix. Furthermore, there was no significant drug adsorption on the surface of the nanofibers. GS release was slow from the scaffold at pH 7.4 where only 36.92±0.07% of total bound GS sulfate was released in 12 hr. At acid and basic pH levels release was 90.67±0.55 and 74.35±1.41% respectively.

3.4*In vitro* antibacterialactivity of scaffold

The antibacterial activity of the composite nanofibrous was performed in solid medium and the results are represented in Figure 4 B-C. The composite nanofibrous scaffolds were able to effectively inhibit bacterial growth as seen in SEM Figure 4.B entrapped *S. aureus* with shrunken morphology compare with untreated bacterial shown on flat poly-L-lysinecoated substrates in supporting Figure S1. The zones of inhibition was found to be 37 mm once the scaffold was placed on Luria broth(LB) agar plate. This result suggested the nanofibrous scaffold had a good bacterial inhibition efficacy under the studied conditions. In contrast, composite nanofibrous scaffolds lacking GSencapsulation did not inhibit the bacterial growth, suggesting that the bacterial inhibition effect is solely related to the encapsulatedGS. Hence, the GSloaded nanofibrous scaffolds were bactericidal to the testing microorganism dueto the strong antibacterial ability of the drug. The results indicate that the Eudragit RL/RS 100 nanofibrous scaffolds possess efficient antibacterial property and can be effectively used in thetreatment of wound healing or dermal bacterialinfections; thereby proving a potential application for use as drug carrier and as a wound dressing agent.Pure GSpowder, as a positive control, was capable of nearly complete inhibition (98.73 ± 0.68%) of the bacterial growth at a concentration of 5 mg/ml. The composite nanofibrous scaffolds exhibited 96.41 ± 0.54% inhibition of bacterial growth. In contrast, the test tube containing bacterial culture without drug loaded scaffold did not showed any reduction in bacterial growth. Thus, the drug loaded scaffold showed near about the same antibacterial activity as the pure GS powder. On the basis of these results, it can be concluded that antibacterial activity of the composite nanofibrous scaffold is comparable to that of the pure GS powder.

3.5*In vivo* wound healing activity in C57/BL6 diabetic mice

Animals with diabetic symptoms were subjected to wound-healing treatments with the rhEGF-nanofibrous scaffolds and controls. The wound area was measured daily for 12 days. The results are shown in Figure 5. A–B, which revealed rhEGF immobilized Eudragit RL/RS 100

nanofibrous scaffolds significantly increased the wound closure rates compared to other treatments. Specifically, the animals with Eudragit RL/RS 100 nanofibrous scaffolds with rhEGF and GS showed 14.31 ± 2.61% open wound area on the 4th day, 10.76 ± 1.92 % open wound area on the 8th day, and 8.91 ± 1.95% open wound area on the 12th day, which were much lesser than other treatments. The Eudragit RL/RS 100 scaffolds with GS and rhEGF both showed more rapid wound closure rates as compared to the scaffolds with only GS and without rhEGF or to the treatment with pure GS ointment. Therefore, it can be concluded that, the rhEGF in the rhEGF immobilized scaffolds is responsible for accelerated wound healing rates at the initial stage of the healing process. **Discussion**

Delayed wound healing due to compromised pathophysiology in diabetic patients is a major challenge for clinicians. Diabetic ulcers are appearing as worldwide health and economic problem, as the number of patients with high morbidity and risk of amputations are continuously increasing. One of the major apprehensions for clinicians in the field of diabetic wound care is the presence of microbial overload at the wound site, which is responsible for causing infections and hence poor wound healing. In view of these challenging circumstances, the present study was aimed to develop nanoengineered carrier devices with the objective of improving the compromised wound healing in diabetic patients.TheGS loadedelectrospun nanofibrous scaffolds were fabricated and immobilized with rhEGF with the objective to determine their (a) physicochemical and biological characterization, (b) i*n vitro* antibacterial activity and(c) *in vivo* wound healing capacity in diabetic mice.

To fulfill the objectives, the GS loaded three-dimensional porous nanofibrous scaffolds were developed using Eudragit RL/RS 100 polymers through electrospinning technique. Thereafter, the scaffolds were modified with rhEGF using the covalent immobilization. The immobilization efficiency was40.7% and is comparable with the reported values in literaure[35].. The physicochemical characterization revealed that the developed biomimetic scaffolds qualitativelyresembled the morphology and prorous structureof thebiological extracellular matrix, which makes them useful as wound healing scaffold. rhEGFimmobilization will promote thecell adhesion and proliferationto scaffolds, and ultimately tissue regeneration.Moreover, the nanofibrous scaffolds were able to form a stable colloidal layered structure in aqueous solution, which facilitated drug encapsulation as shown in the XRD spectra. In amorphous materials, X-

rays will be scattered in many directions leading to a large bump distributed in a wide range (2 Theta) instead of high intensity narrower peaks. Appearance of the broad peaks in the 2θ = 5-25º region was attributed to the amorphous nature of the Eudragit RL/RS 100 polymer. The occurrence of characteristic peak ofGS in the XRD spectra indicated the presence of the drug. The XRD data suggested that the incorporation of GS within polymer is primarily via the drug intercalation within the polymer interlayer space. It is also possible that a small portion of GScan be adsorbed onto the polymer surface via hydrogen bonding or other weak forces.

TGA curves showed that the weight loss of GS and pure polymers started at lower temperature compared to the GS loaded scaffolds; therefore showing imporvedthermal stability of both the composite scaffolds in comparison to pure GS or polymers alone. The most likely reason for the increase in thermal stability of the nanofibrous scaffolds may be the decrease in the labile oxygen containing functional group due to covalent bonding between GS and nanofibrous scaffolds[36]. Furthermore, the gradual 40%weight loss below 260–350ºC is likely due to the loss of residual functional group on the GS loaded scaffolds. Additionally, the DSC thermograms indicated that the stability was increased due to encapsulation of drug between polymeric chains. The results suggest that biomimetic morphology and improved crystallinity observed here could be useful for the extended storage of the scaffolds.The swelling indices of the developed scaffolds were favorable to be used in wound dressings to absorb excess exudates even from wounds s[37,38].The porosity of the scaffolds should be high enough for efficient tissue repair during wound healing because the microscale and nanoscale porous structure allow passage and exchange of nutrients and gases, which are important for cellular growth and tissue regeneration[39].Particularly, the preferred porosity should be in the range of 60-90%. [40]The water contact angle of the scaffolds indicated the improved hydrophilicity of nanofibrous scaffolds for increasing their cell adhesion ability.Generally, if the water contact angle is smaller than 90°, the solid surface is consideredhydrophilic and wettableand if the water contact angle is larger than 90°, the solid surface is considered hydrophobic and not wettable[41].

The encapsulationGS into nanofibrous scaffolds was achieved with an entrapment efficiency of 72.2±0.74 %. The reason for comparatively lower entrapment efficiency may be that since Eudragit RL/RS 100 is a low molecular weight polymer, so it entraps smaller amount of active substance than higher molecular weight polymers. Additionally, the drug loading capacity was as

high as 2.79 ± 0.06 µg mg $^{-1}$. These results are in accordance with the assumption that since a high drug loading implies the polymer to drug ratio will be low, and the polymer present will not be sufficient to fully entrap the drug, resulting in lower entrapment efficiency.Sustained releasewas observed in the *in vitro* drug release studies. Further, it was seen that the cumulative percentage release of drug did not reach 100% during 12 hours. This could probably be explained by the fact the scaffold still retained somewhat its original shape and showed less visible signs of degradation up till the point the experiment was concluded (12 hours). As such the drug could still be trapped in the scaffolds and not be released. More explicitly, the release at pH 3 and pH 9 is much higher than that released at pH 7.4. This is so because the hydrogen bonding interaction between GS and the nanofibrous scaffolds is strongest at the neutral pH.

The *in vitro* antibacterial activities of the developed nanofibrous scaffolds were confirmed against *Staphylococcus aureus* bacteria, which is commonly found in diabetic wounds and used as pathogenic bacterial model for *in vitr*o antibacterial efficacy[42-44]. The released antibiotic was able to inhibit the growth of bacteria.The results indicate that the drug encapsulation does not influences the release and bactericidal properties of GSIn the *in vivo* wound healing studies conducted in C57/BL6 mice, the rhEGF nanofibrous scaffolds significantly increased the wound closure rates compared with other treatmentsduring the initial stages of the healing process.Particularly, the Eudragit RL/RS 100 scaffolds with GS and rhEGF both showed more rapid wound closure rates as compared to the scaffolds with only GS /without rhEGF or to the treatment with pure GS ointment. Hence, it could be concluded that the presence of rhEGF in the scaffolds is responsible for accelerated wound healing rates at the initial stage of the healing process.

4. Conclusions

These scaffolds have a promising potential as therapy in treating antibacterial diabetic wounds and as wound healing material, which would on one end, permit optimal interaction between tissue and healing material, given the nanoscale topography. On the other hand, GS entrapment

and rhEGF immobilization would assist as a reservoir for controlled release of GS and rhEGF, preventing furtherbacterial infection challenges and hastening the wound healing process. The results obtained are promising, since the benefits of delivering bioactive molecules within a dual carrier material to inactivate bacteria in diabetic wounds and simultaneously quicken wound healing were clearly shown, and can enhance the applicability of delivery systems in wound healing applications. The protocol developed in the current study may serve as a template for developing other next generation smart wound healing regenerative scaffolds to improve quality of life in debilitating diseases[45-47].

There is a great necessity for the use of scaffolds which maintain the specific phenotypic characteristics of the cells as most of most cells are not able to form fully viable 3-D tissue. Till now only few *in vivo* studies have shown the medical and clinical aspects of scaffolds. Therefore creating new scaffolds with advanced clinical properties is a must. Research still focuses on the maintenance of the biological activity of the growth factors. Their protein conformation and hence the biological activity and therapeutic potential is a major challenge that needs to be accounted for. Another factor that needs special consideration is the degradation of the polymer at a controlled rate. The degradation into non-toxic end products deserves special attention. Mechanical and physical properties like structure and arrangement of fibers need to be addressed. Another field of research deals with the process of electrospinning and the need to integrate it with other scientific fields to expand and elaborate the commercial and biomedical applications of nanofibrous scaffolds. Stem cells are an important material for tissue engineering and can play a significant role as a cellular therapy in the development of wound care materials. Extensive research is therefore needed to elucidate the differentiation potential of stem cells. In the future, new insights could be gained regarding the interactions of growth factors and cytokines at the cellular level. Further developments could provide the technology for the replacement of the damaged tissue with a complete organ.

Conflict of interest

The authors confirm that this article content has no conflict of interest.

Acknowledgements

CharuDwivedigratefully acknowledges The Council of Scientific and Industrial Research (CSIR), Ministry of HRD, Government of India for CSIR-SRF Fellowship support.We thank TheNational Centre of Laboratory Animal Sciences (National Institute of Nutrition-ICMR), Hyderabad providing the C57/BL6 mice. AVS thank Maxplanck Society for funding and grass root program. AVS thanks toMaduBatuwangalafor proof reading the manuscript draft.

REFERENCES.

1. Tsourdi E, Barthel A, Rietzsch H, Reichel A, Bornstein SR. Current aspects in the pathophysiology and treatment of chronic wounds in diabetes mellitus. BioMed research international 2013;2013.
2. Badr G, Badr BM, Mahmoud MH, Mohany M, Rabah DM, Garraud O. Treatment of diabetic mice with undenatured whey protein accelerates the wound healing process by enhancing the expression of MIP-1α, MIP-2, KC, CX3CL1 and TGF-β in wounded tissue. BMC immunology 2012;13(1):32.
3. Rosique RG, Rosique MJ, Farina Junior JA. Curbing inflammation in skin wound healing: a review. International journal of inflammation 2015;2015.
4. Singh AV, Subhashree L, Milani P, Gemmati D, Zamboni P. Interplay of iron metallobiology, metalloproteinases, and FXIII and role of their gene variants in venous leg ulcer. The international journal of lower extremity wounds 2010:1534734610384653.
5. White R, McIntosh C. Topical therapies for diabetic foot ulcers: standard treatments. J Wound Care 2008;17(10):426-32.
6. Jannesari M, Varshosaz J, Morshed M, Zamani M. Composite poly (vinyl alcohol)/poly (vinyl acetate) electrospun nanofibrous mats as a novel wound dressing matrix for controlled release of drugs. Int J Nanomedicine 2011;6:993-1003.
7. Spichler A, Hurwitz BL, Armstrong DG, Lipsky BA. Microbiology of diabetic foot infections: from Louis Pasteur to 'crime scene investigation'. BMC medicine 2015;13(1):2.
8. Trivedi U, Parameswaran S, Armstrong A, Burgueno-Vega D, Griswold J, Dissanaike S, Rumbaugh KP. Prevalence of multiple antibiotic resistant infections in diabetic versus nondiabetic wounds. Journal of pathogens 2014;2014.
9. Singh AV, Raymond M, Pace F, Certo A, Zuidema JM, McKay CA, Gilbert RJ, Lu XL, Wan LQ. Astrocytes increase ATP exocytosis mediated calcium signaling in response to microgroove structures. Scientific reports 2015;5.
10. Andreu V, Mendoza G, Arruebo M, Irusta S. Smart dressings based on nanostructured fibers containing natural origin antimicrobial, anti-inflammatory, and regenerative compounds. Materials 2015;8(8):5154-5193.
11. Singh AV, Gailite L, Vyas V, Lenardi C, Forti S, Matteoli M, Milani P. Rapid prototyping of nano- and micro-patterned substrates for the control of cell neuritogenesis by topographic and chemical cues. Materials Science and Engineering: C 2011;31(5):892-899.
12. Dwivedi C, Pandey H, C Pandey A, W Ramteke P. Nanofibre based smart pharmaceutical scaffolds for wound repair and regenerations. Current pharmaceutical design 2016;22(11):1460-1471.

13. V Singh A, K Mehta K. Top-down versus bottom-up nanoengineering routes to design advanced oropharmacological products. Current pharmaceutical design 2016;22(11):1534-1545.
14. Singh AV. Biotechnological applications of supersonic cluster beam-deposited nanostructured thin films: Bottom-up engineering to optimize cell–protein–surface interactions. Journal of Biomedical Materials Research Part A 2013;101(10):2994-3008.
15. Singh AV, Maheshwari S, Giovanni D, Naikmasur VG, Rai A, Aditi A, Gade W, Vyas V, Gemmati D, Zeri G. Nanoengineering approaches to design advanced dental materials for clinical applications. Journal of Bionanoscience 2010;4(1-2):53-65.
16. Zhang L, Gu F, Chan J, Wang A, Langer R, Farokhzad O. Nanoparticles in medicine: therapeutic applications and developments. Clinical pharmacology and therapeutics 2008;83(5):761-769.
17. Abdel-Wahhab MA, Márquez F. Nanomaterials in Biomedicine. Scientific Research Publishing; 2015.
18. Singh AV, Patil R, Lenardi C, Milani P and Gade W. N. . Nanobiomaterial Applications in Tissue Repair and Ulcer Management: A New Role for Nanomedicine. In: Kumar S. A TSaWS-F, editor. Biocompatible Nanomaterials: Synthesis, Characterization and Applications: Nova Science Publishers.; 2011. p 117-141.
19. Duan H, Feng B, Guo X, Wang J, Zhao L, Zhou G, Liu W, Cao Y, Zhang WJ. Engineering of epidermis skin grafts using electrospun nanofibrous gelatin/polycaprolactone membranes. Int J Nanomedicine 2013;8(2):2077-2084.
20. Shen X, Yu D, Zhu L, Branford-White C, White K, Chatterton NP. Electrospun diclofenac sodium loaded Eudragit® L 100-55 nanofibers for colon-targeted drug delivery. International journal of pharmaceutics 2011;408(1):200-207.
21. Rošic R, Kocbek P, Pelipenko J, Kristl J, Baumgartner S. Nanofibers and their biomedical use. Acta pharmaceutica 2013;63(3):295-304.
22. Beachley V, Wen X. Polymer nanofibrous structures: Fabrication, biofunctionalization, and cell interactions. Progress in polymer science 2010;35(7):868-892.
23. Tığlı RS, Kazaroğlu NM, Mavış B, Gümüşderelioğlu M. Cellular behavior on epidermal growth factor (EGF)-immobilized PCL/gelatin nanofibrous scaffolds. Journal of Biomaterials Science, Polymer Edition 2011;22(1-3):207-223.
24. Singh AV, Subhashree L, Milani P, Gemmati D, Zamboni P. Review: Interplay of Iron Metallobiology, Metalloproteinases, and FXIII, and Role of Their Gene Variants in Venous Leg Ulcer. The International Journal of Lower Extremity Wounds 2010;9(4):166-179.
25. Singh AV, Vyas V, Maontani E, Cartelli D, Parazzoli D, Oldani A, Zeri G, Orioli E, Gemmati D, Zamboni P. Investigation of in vitro cytotoxicity of the redox state of ionic iron in neuroblastoma cells. Journal of neurosciences in rural practice 2012;3(3):301.
26. Meng Z, Xu X, Zheng W, Zhou H, Li L, Zheng Y, Lou X. Preparation and characterization of electrospun PLGA/gelatin nanofibers as a potential drug delivery system. Colloids and Surfaces B: Biointerfaces 2011;84(1):97-102.
27. Fouad H, Elsarnagawy T, Almajhdi FN, Khalil KA. Preparation and in vitro thermo-mechanical characterization of electrospun PLGA nanofibers for soft and hard tissue replacement. Int J Electrochem Sci 2013;8:2293-2304.
28. Dwivedi C, Pandey H, Pandey AC, Ramteke PW. NOVEL GENTAMICIN LOADED ELECTROSPUN NANOFIBROUS SCAFFOLDS FOR WOUND HEALING: AN IN-VITRO STUDY. International Journal of Pharmaceutical Sciences and Research 2013;4(6):2230.
29. Dwivedi C, Pandey H, C Pandey A, W Ramteke P. Fabrication and Assessment of Gentamicin Loaded Electrospun Nanofibrous Scaffolds as a Quick Wound Healing Dressing Material. Current Nanoscience 2015;11(2):222-228.

30. Singh AV, Batuwangala M, Mundra R, Mehta K, Patke S, Falletta E, Patil R, Gade W. Biomineralized anisotropic gold microplate–macrophage interactions reveal frustrated phagocytosis-like phenomenon: a novel paclitaxel drug delivery vehicle. ACS applied materials & interfaces 2014;6(16):14679-14689.
31. Wang S, Zheng F, Huang Y, Fang Y, Shen M, Zhu M, Shi X. Encapsulation of amoxicillin within laponite-doped poly (lactic-co-glycolic acid) nanofibers: preparation, characterization, and antibacterial activity. ACS applied materials & interfaces 2012;4(11):6393-6401.
32. Singh AV, Sitti M. Patterned and Specific Attachment of Bacteria on Biohybrid Bacteria-Driven Microswimmers. Advanced healthcare materials 2016;5(18):2325-2331.
33. Garg M, Garg BR, Jain S, Mishra P, Sharma RK, Mishra AK, Dutta T, Jain NK. Radiolabeling, pharmacoscintigraphic evaluation and antiretroviral efficacy of stavudine loaded 99mTc labeled galactosylated liposomes. European Journal of Pharmaceutical Sciences 2008;33(3):271-281.
34. Kadnur SV, Goyal RK. Beneficial effects of Zingiber officinale Roscoe on fructose induced hyperlipidemia and hyperinsulinemia in rats. Indian J Exp Biol 2005;43(12):1161-4.
35. Choi JS, Leong KW, Yoo HS. In vivo wound healing of diabetic ulcers using electrospun nanofibers immobilized with human epidermal growth factor (EGF). Biomaterials 2008;29(5):587-596.
36. Vikram Singh A, Gharat T, Batuwangala M, Park BW, Endlein T, Sitti M. Three-dimensional patterning in biomedicine: Importance and applications in neuropharmacology. J Biomed Mater Res B Appl Biomater 2017.
37. Pal K, Banthia AK, Majumdar DK. Polyvinyl alcohol–glycine composite membranes: preparation, characterization, drug release and cytocompatibility studies. Biomedical Materials 2006;1(2):49.
38. Yu H, Xu X, Chen X, Hao J, Jing X. Medicated wound dressings based on poly (vinyl alcohol)/poly (N-vinyl pyrrolidone)/chitosan hydrogels. Journal of Applied Polymer Science 2006;101(4):2453-2463.
39. Murugan R, Ramakrishna S. Nano-featured scaffolds for tissue engineering: a review of spinning methodologies. Tissue engineering 2006;12(3):435-447.
40. Chong E, Phan T, Lim I, Zhang Y, Bay B, Ramakrishna S, Lim C. Evaluation of electrospun PCL/gelatin nanofibrous scaffold for wound healing and layered dermal reconstitution. Acta biomaterialia 2007;3(3):321-330.
41. Singh AV, Baylan S, Park BW, Richter G, Sitti M. Hydrophobic pinning with copper nanowhiskers leads to bactericidal properties. PLoS One 2017;12(4):e0175428.
42. Singh AV, Vyas V, Patil R, Sharma V, Scopelliti PE, Bongiorno G, Podesta A, Lenardi C, Gade WN, Milani P. Quantitative characterization of the influence of the nanoscale morphology of nanostructured surfaces on bacterial adhesion and biofilm formation. PLoS One 2011;6(9):e25029.
43. Singh AV, Vyas V, Salve TS, Cortelli D, Dellasega D, Podestà A, Milani P, Gade W. Biofilm formation on nanostructured titanium oxide surfaces and a micro/nanofabrication-based preventive strategy using colloidal lithography. Biofabrication 2012;4(2):025001.
44. Singh AV, Galluzzi M, Borghi F, Indrieri M, Vyas V, Podestà A, Gade W. Interaction of bacterial cells with cluster-assembled nanostructured titania surfaces: An atomic force microscopy study. Journal of nanoscience and nanotechnology 2013;13(1):77-85.
45. Khare M, Singh A, Zamboni P. Prospect of brain-machine interface in motor disabilities: the future support for multiple sclerosis patient to improve quality of life. Ann Med Health Sci Res 2014;4(3):305-12.
46. Singh AV. Recent Trends in Nano-Biotechnology Reinforcing Contemporary Pharmaceutical Design. Curr Pharm Des 2016;22(11):1415-7.
47. Singh AV. Multiple sclerosis takes venous route: CCSVI and liberation therapy. Indian J Med Sci 2010;64(7):337-40.

Figure captions

Figure 1. Schematic illustration of fabrication of 3D electrospun nanoscaffolds and subsequent modification with rhEGF and antibiotic gentamycin.

Figure 2. Physicochemical characterization. (A) SEM micrographs of composite nanofibrous scaffolds (insert graph shows average nanofiber size distribution). (B) Attenuated Total Reflection IR spectra of GS and rhEGF supplemented eudragit RL/RS 100 scaffold showing assigned vibrational/stretching frequencies of different functional groups. (C) XRD spectra of composite nanoscaffolds.

Figure 3. Thermal properties and wettability of the 3D scaffolds. (A) TGA curves of Eudragit RL/RS 100, composite nanoscaffolds and GS. (B) DSC curves of 3D composite nanoscaffolds and GS. (C) Comparison of porosity and swelling index of composite nanoscaffolds and cotton gauze, and (D) Water contact angle value for composite nanofibrous scaffold.

Figure 4. Controlled release and characterization of antibacterial properties. (A) Release kinetics of GS on composite nanofibrous scaffold at different pH values. (B) SEM image showing GS

mediated killing of *Staphylococcus aureus* trapped inside 3D scaffold. (C) Antibacterial activity of composite in solid LB-agar media (scaffold; control). Red circle is drawn to attract attention to visualize zone of inhibition. (D) Graph showing antimicrobial efficacy of nanofibrous scaffold against *S. aureus* in terms of log reduction of cfu/mL in LB liquid medium.

Figure 5. Wound healing in diabetic C57/BL6 mice after treatment with various electrospun nanofibrous scaffolds,*(panels from left to right represent the extent of wound healing during12 days period).* Group 1 – No treatment (negative control);Group 2 – 0.1% gentamicinsulphate ointment (positive control); Group 3 - Eudragit RL/RS 100 scaffold without gentamicinsulphate and rhEGF ; Group 4 - Eudragit RL/RS 100 scaffold with gentamicin sulphate and rhEGF;Group 5 – Eudragit RL/RS 100 scaffold with gentamicin sulphate and without rhEGF. (B) Open wound area (% of initial area) over 12 days for each treatment group.The data presented is the mean ± S.D. for 6 mice per group, *$p<0.001$ and **$p<0.001$ indicates statistical significance compared to the control.

Table 1. Electrospinning parameters for 3D scaffold fabrication

DC Voltage	16 kV
Flow rate	0.5 ml per hour
Inner Hole Diameter	0.9 mm
Tip to Collector Distance	10 cm

Table 2: Interpretation of the ATR-IR spectrum of rhEGF and gentamycin sulphate loaded eudragit nanofibrous scaffolds

Assigned IR peak (cm^{-1})	*Type of vibrations (groups)*
3600-4000	Water vapors
3450	-OH vibration from H_2O
3500	-NH stretching from Amides
2980	Asymmetric -CH_3 stretching
2073	Nonspecific peaks originating from C=O and CO in medium
1731	Symmetry methyl (Ch3) bending from rhEGF
1644	Amide I from rhEGF
1536	Amide II from rhEGF
1381	asymmetric stretching vibration from -SO_2 (GS)
1245	asymmetric stretching from -PO_2 (rhEGF)
1158	C-O (H) stretching
1050	-PO_2 vibrations

Table 3. Polymer drug parameters

Polymer-Drug Parameters	*Percentage (± standard deviation)*
Drug Entrapment Efficiency	72.2± 0.74
Drug Loading Capacity	2.79± 0.06
Release at pH 3.0	90.67± 0.55

Release at pH 7.4	36.92± 0.07
Release at pH 9.0	74.35± 1.41

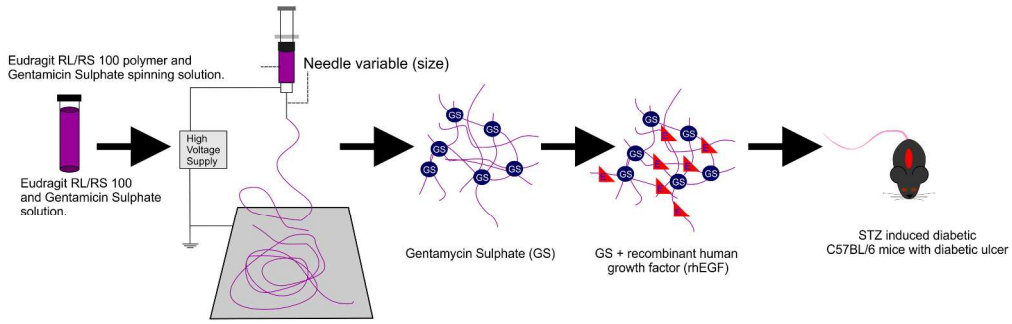

Figure 1. Schematic illustration of fabrication of 3D electrospun nanoscaffolds and subsequent modification with rhEGF and antibiotic gentamycin.

282x89mm (300 x 300 DPI)

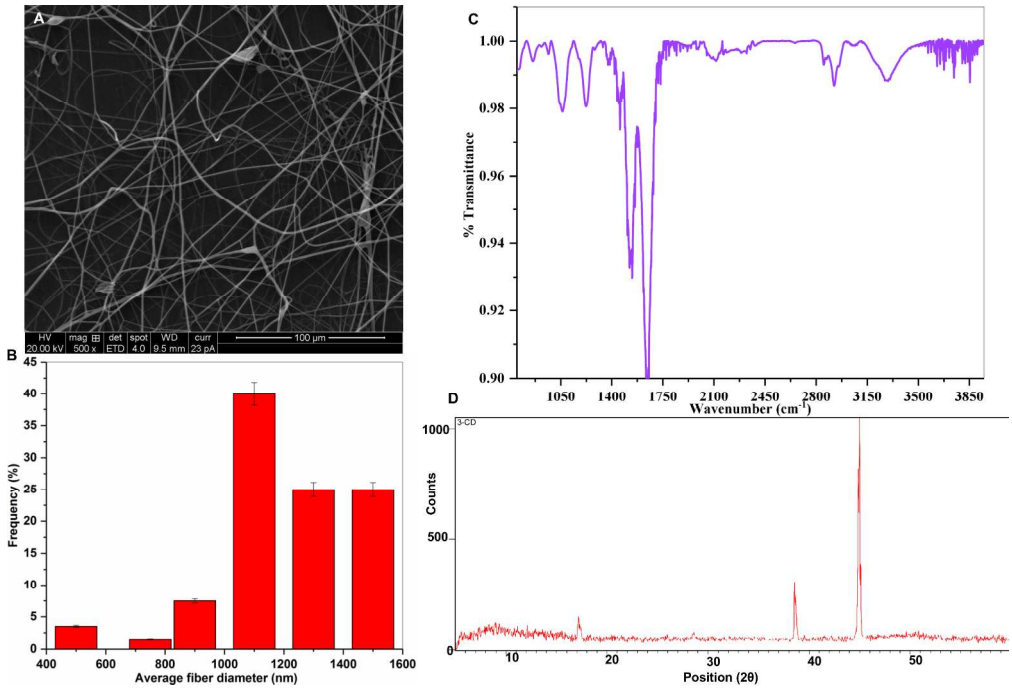

Figure 2. Physicochemical characterization. (A) SEM micrographs of composite nanofibrous scaffolds. (B) graph shows average nanofiber size distribution. (C) Attenuated Total Reflection IR spectra of GS and rhEGF supplemented eudragit RL/RS 100 scaffold showing assigned vibrational/stretching frequencies of different functional groups. (D) XRD spectra of composite nanoscaffolds.

280x190mm (300 x 300 DPI)

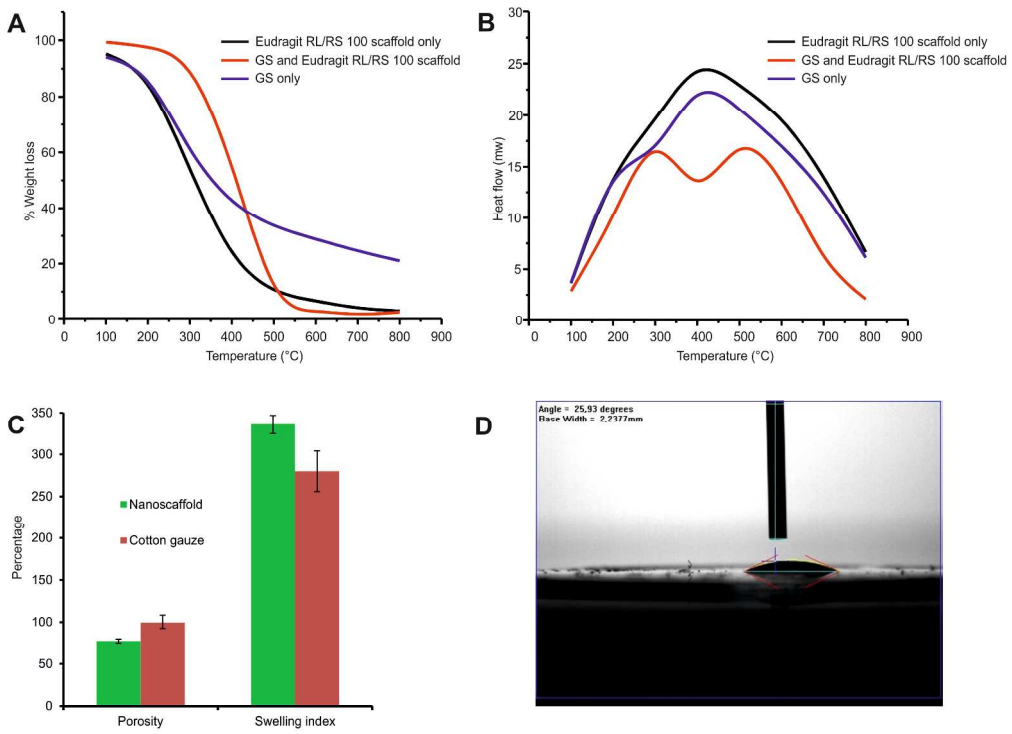

Figure 3. Thermal properties and wettability of the 3D scaffolds. (A) TGA curves of Eudragit RL/RS 100, composite nanoscaffolds and GS. (B) DSC curves of 3D composite nanoscaffolds and GS. (C) Comparison of porosity and swelling index of composite nanoscaffolds and cotton gauze, and (D) Water contact angle value for composite nanofibrous scaffold.

279x201mm (300 x 300 DPI)

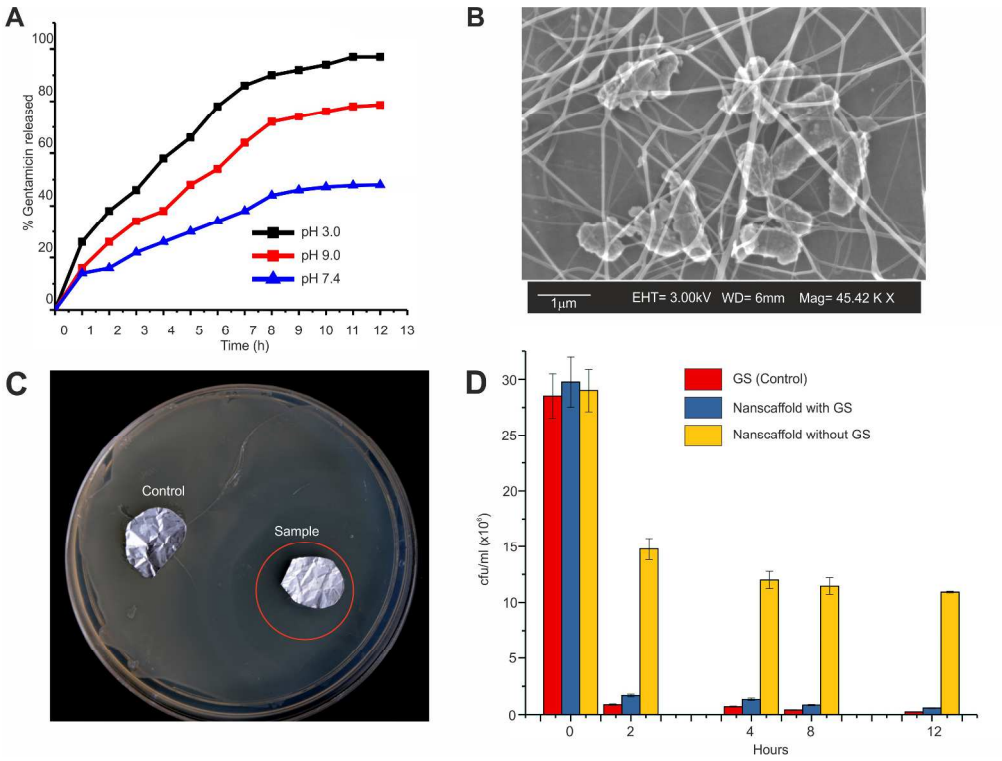

Figure 4. Controlled release and characterization of antibacterial properties. (A) Release kinetics of GS on composite nanofibrous scaffold at different pH values. (B) SEM image showing GS mediated killing of Staphylococcus aureus trapped inside 3D scaffold. (C) Antibacterial activity of composite in solid LB-agar media (scaffold; control). Red circle is drawn to attract attention to visualize zone of inhibition. (D) Graph showing antimicrobial efficacy of nanofibrous scaffold against S. aureus in terms of log reduction of CFU/mL in LB liquid medium.

267x200mm (300 x 300 DPI)

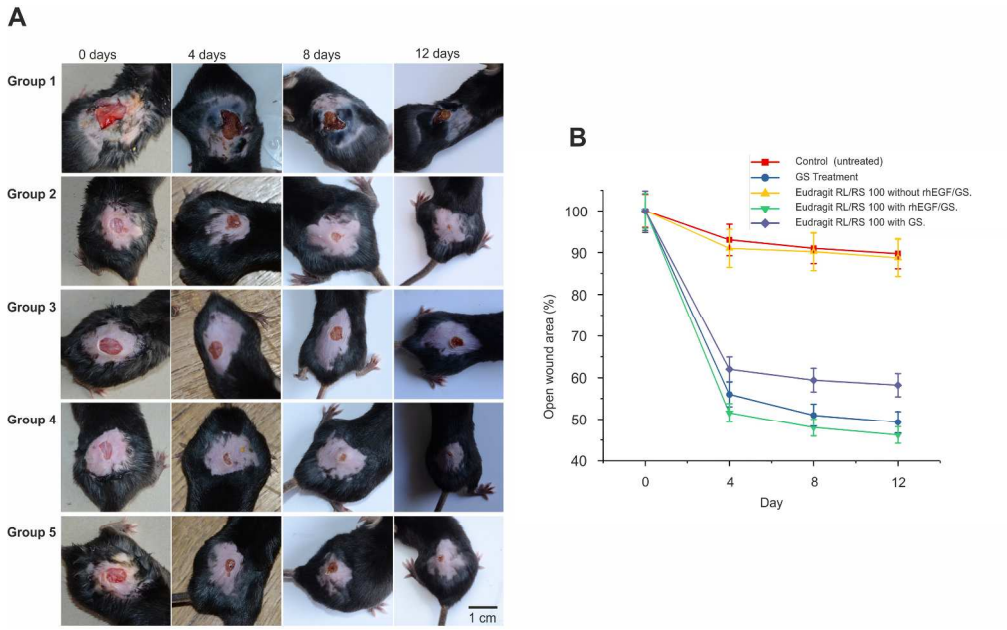

Figure 5. Wound healing in diabetic C57/BL6 mice after treatment with various electrospun nanofibrous scaffolds, (panels from left to right represent the extent of wound healing during 12 days period). Group 1 – No treatment (negative control); Group 2 – 0.1% gentamicin sulphate ointment (positive control); Group 3 - Eudragit RL/RS 100 scaffold without gentamicin sulphate and rhEGF ; Group 4 - Eudragit RL/RS 100 scaffold with gentamicin sulphate and rhEGF; Group 5 – Eudragit RL/RS 100 scaffold with gentamicin sulphate and without rhEGF. (B) Open wound area (% of initial area) over 12 days for each treatment group.

277x172mm (300 x 300 DPI)